Volume 1 | Number 1 | Jan 2013 | Pages 1–100

ChemComm

Chemical Communications
www.rsc.org/chemcomm

ROYAL SOCIETY OF CHEMISTRY

This is an *Accepted Manuscript*, which has been through the Royal Society of Chemistry peer review process and has been accepted for publication.

Accepted Manuscripts are published online shortly after acceptance, before technical editing, formatting and proof reading. Using this free service, authors can make their results available to the community, in citable form, before we publish the edited article. We will replace this *Accepted Manuscript* with the edited and formatted *Advance Article* as soon as it is available.

You can find more information about *Accepted Manuscripts* in the **Information for Authors**.

Please note that technical editing may introduce minor changes to the text and/or graphics, which may alter content. The journal's standard **Terms & Conditions** and the **Ethical guidelines** still apply. In no event shall the Royal Society of Chemistry be held responsible for any errors or omissions in this *Accepted Manuscript* or any consequences arising from the use of any information it contains.

Journal Name

COMMUNICATION

An efficient planar-heterojunction solar cell based on wide-bandgap CH₃NH₃PbI₂.₁Br₀.₉ perovskite film for tandem cell application

Weidong Zhu,[a] Chunxiong Bao,[a] Faming Li,[a] Xiaoxin Zhou,[a] Jie Yang,[a] Tao Yu,*[abc] and Zhigang Zou[abc]

A dense and homogenous flat wide-bandgap (1.75 eV) CH₃NH₃PbI₂.₁Br₀.₉ perovskite film was prepared via a facile halide exchange route. The planar-heterojunction solar cell showed the optimal power conversion efficiency of 12.67% with negligible current hysteresis benefited from the film's large grains and vertically oriented grain boundaries.

Organolead trihalide perovskites-based solar cells as a new kind of photovoltaic (PV) technology have drawn exceptional attention in the past few years owing to their rapidly increased power conversion efficiency (PCE) and low-cost prospectus in terms of raw materials and device fabrication.[1-3] The organolead trihalide perovskites are the most key parts in the cells.[4] The investigations focused on these perovskite films have revealed their rather outstanding optical and electrical properties including high absorption coefficient,[4] long carrier diffusion lengths,[5] and ambipolar charge transport,[6] which are vital for highly performing solar cells. Furthermore, the attractive feature is their favorably band-gap tunability ranged from about 1.55 to 2.28 eV, by appropriate halide substitutions.[7-9] This property points out the potential applications of organolead trihalide perovskites for high-efficiency tandem solar cells in conjunction with the state-of-the-art PV technologies, even for all perovskite tandem solar cells.[7]

The most important aspect of designing tandem solar cells is to select light absorption materials with suitable bandgaps to optimize harvesting of solar spectrum.[10] In particular, for inexpensive two-cell tandem modules, Si or band-gap-tunable III-V semiconductors is preferred for the bottom cell, and the top-cell material should have a bandgap of 1.75~1.80 eV.[11, 12] Based on this, some exploring works have

been done. For example, by employing one-step spin-coated MAPbI₂Br with a band-gap of ~1.77 eV, Zhang et al. realized a device with a PCE of 6.64%.[13] Wang et al. also prepared MAPbI₂Br based solar cells with the TiO₂/Al₂O₃/carbon architecture. An appreciable PCE of 11.03% was achieved.[14] However, all the devices in these works were mesoscopic structure, which is relatively difficult for incorporation (especially as the top cell) to build tandem devices compared to planar cell structure.[7] The reasons for the initial works mainly focused on mesoscopic device is that planar perovskite solar cells require high-quality perovskite films with uniform substrate coverage,[2] but the well-developed methods for realizing high-quality MAPbI₃ films does not yield the MAPbI₃₋ₓBrₓ films with similar quality.[8, 15, 16] For example, Huang et al. synthesized the MAPbI₂.₄Br₀.₆ films via solvent annealing-induced interdiffusion method performed well in preparing high-quality MAPbI₃ films.[17] Yet, the devices with the MAPbI₂.₄Br₀.₆ films showed relatively low PCE, which was mainly attributed to high trap densities resulted from the inferior film quality. A layer of spun fullerene derivatives on the top of perovskite layer was essential to passive the traps and boost the device performance, which partly perplexes the device structure. When using the MACl as additive in MAPbI₂Br precursor to realize planar device as reported by Zhu et al., the MAPbI₂Br easily formed nanosheet-like morphology,[7] which unavoidable contains more grain boundaries and intragranular defects. Thus, developing a facile synthetic approach for preparing high-quality MAPbI₃₋ₓBrₓ films with the bandgap within 1.75~1.80 eV would facilitate the development of perovskite-based tandem cells.

In this communication, we present a facile and effective halide exchange route to grow dense and homogenous flat MAPbI₂.₁Br₀.₉ film with wide bandgap of 1.75 eV by topologic transforming interdiffusion grown MAPbI₃ film. This MAPbI₂.₁Br₀.₉ film composes of large grains and vertically oriented grain boundaries, thus significantly reducing the nonradiative recombination and improving the dissociation property of charge carriers. The planar-heterojunction solar cell based on this high-quality wide-bandgap MAPbI₂.₁Br₀.₉ film

[a.] *National Laboratory of Solid State Microstructures & Eco-Materials and Renewable Energy Research Center (ERERC) at Department of Physics, Nanjing University, Nanjing 210093, P. R. China. E-mail: yutao@nju.edu.cn.*
[b.] *Collaborative Innovation Center of Advanced Microstructures, Nanjing University, Nanjing 210093, P. R. China..*
[c.] *Jiangsu Key Laboratory for Nano Technology, Nanjing 210093, P. R. China.*
†Electronic Supplementary Information (ESI) available: See
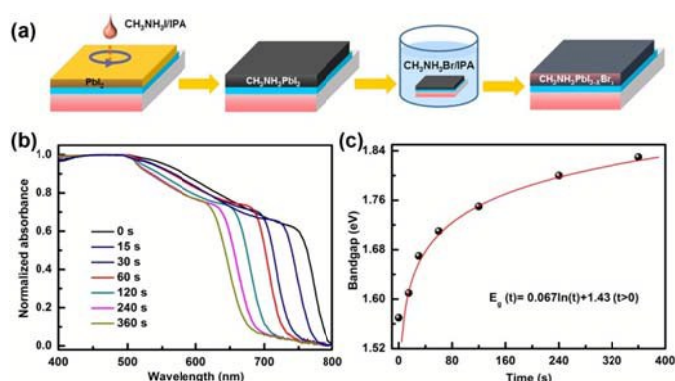DOI: 10.1039/x0xx00000x

Fig. 1 (a) Schematic process for the preparation of $MAPbI_{3-x}Br_x$ film by halide exchange. (b) Normalized UV-vis absorption spectra of $MAPbI_{3-x}Br_x$ films prepared with various halide exchange time. (c) A logarithmic relationship between the estimated bandgap values of the $MAPbI_{3-x}Br_x$ films and halide exchange time.

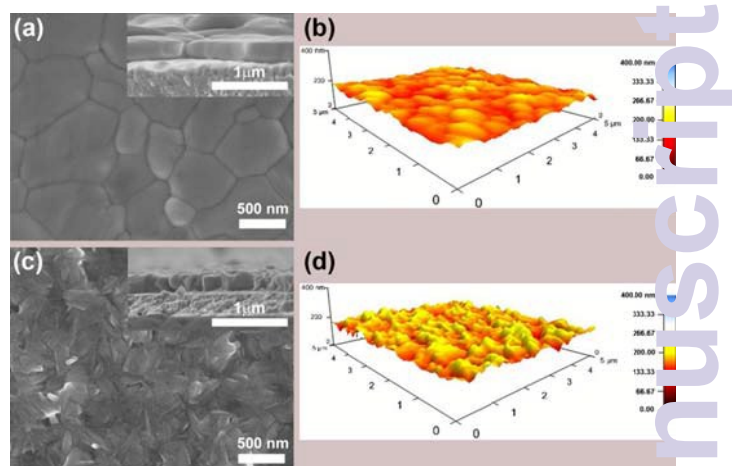**Fig. 2** The surficial SEM images of $MAPbI_{2.1}Br_{0.9}$ films prepared by halide exchange (a) and solvent annealing-induced interdiffusion process (c). The inserts gives the corresponding cross-sectional SEM images. (b) and (d) AFM topographical images of $MAPbI_{2.1}Br_{0.9}$ films prepared by halide exchange and solvent annealing-induced interdiffusion process.

showed an optimal PCE of 12.67% with negligible current hysteresis, which is much better than that of the device employed interdiffusion grown $MAPbI_{2.1}Br_{0.9}$ film with the same bandgap.

Fig. 1(a) shows the schematical processes for preparation of $MAPbI_{3-x}Br_x$ film via halide exchange route. Firstly, $MAPbI_3$ parent film was fabricated by solvent annealing-induced interdiffusion method. Then, the $MAPbI_3$ film was dipped into 5 mg mL^{-1} MABr solution in isopropyl alcohol (IPA) for a fixed duration to realize halide exchange. Finally, the film was baked at 95 °C for 15 min (the detailed film and device fabrication processes can be found in Supporting Information). We found that the absorption onset of as-fabricated perovskite films showed a continuous blue shift with the increase of halide exchange time, as evidenced in Fig. 1(b), indicating the successful incorporation of Br into $MAPbI_3$.[9, 18] The absorption onset blue-shift can be easily ascribed to the variation of band gap (E_g) of the samples.[9] The corresponding E_g values were estimated using Tauc equation,[19] which exhibit a logarithmic relationship with halide exchange time, as given in Figure 1(c). All the above results indicate that the bandgap of $MAPbI_{3-x}Br_x$ film could be controllably tuned by varying halide exchange time. Especially, when the halide exchange time is to be 120 s, the $MAPbI_{3-x}Br_x$ film with a bandgap of 1.75 eV can be obtained, which perfectly meet the requirement for top-cell material in tandem solar cells.[11] Fig. S1 shows the XRD patterns of the $MAPbI_3$ film prepared by solvent annealing-induced interdiffusion process and the $MAPbI_{3-x}Br_x$ film with the bandgap of 1.75 eV. It can be seen that the parent $MAPbI_3$ film showed the major diffraction peaks of orthorhombic perovskite, which is verified by the dominant diffraction peaks at 14.08°, 28.40°, and 31.86°.[1, 2, 4] For the $MAPbI_{3-x}Br_x$ sample, all the XRD peaks shifted to larger diffraction angles, and only one single phase existed, further indicating the successful incorporation of Br into $MAPbI_3$ and the formation of $MAPbI_{3-x}Br_x$ compound.[9, 17, 18] Meanwhile, all the diffraction peaks well match with the cubic Pm3m perovskite phase, which agrees with the previously reported results about $MAPbI_{3-x}Br_x$ film with the same bandgap.[9] Based on the previous reported

relation about the composition of halides in $MAPb(I_{1-x}Br_x)_3$ film and its band-gap value, the chemical formula of the obtained $MAPbI_{3-x}Br_x$ film with the bandgap of 1.75 eV was identified to be $MAPbI_{2.1}Br_{0.9}$.[9, 20]

After determining the halide exchange time to realize $MAPbI_{2.1}Br_{0.9}$ film with a proper bandgap of 1.75 eV (hereinafter abbreviated to HE-$MAPbI_{2.1}Br_{0.9}$), we further investigated the morphology of the obtained film. For comparison, we also prepared $MAPbI_{2.1}Br_{0.9}$ film with the same bandgap via the solvent annealing-induced interdiffusion method reported by Huang et al. (hereinafter abbreviated to SA-$MAPbI_{2.1}Br_{0.9}$).[17] Fig. 2(a) shows the scanning electron microscopy (SEM) images of HE-$MAPbI_{2.1}Br_{0.9}$ film. It can be seen that the surface of HE-$MAPbI_{2.1}Br_{0.9}$ film have full surface coverage and exhibit a dense-grained uniform morphology, with grain sizes ranging from 300 nm to 1 μm. In addition, large oriented-crystalline grains and vertically aligned grain boundaries were clearly identified from a typical cross-sectional SEM image of the film.[21] Such film morphology is quite alike to the parent $MAPbI_3$ film prepared by solvent annealing-induced interdiffusion process, as revealed in Fig. S2.[22] In contrast, SA-$MAPbI_{2.1}Br_{0.9}$ film also has full surface coverage, as shown in Fig. 2(c). Yet the film is composed of randomly cumulated nanorod-like structures, which detrimentally increases the film non-uniformity, as well as simultaneously increases the grain boundaries and defects in the film. The morphology difference between the SA-$MAPbI_{2.1}Br_{0.9}$ film and the parent $MAPbI_3$ film is mainly attributed that the CH_3NH_3Br in the precursor alter the nucleation kinetics of the film,[23] which is consistent with the previous works.[7, 8, 16, 17] The surface roughness of the films was further investigated by atomic force microscopy (AFM), as given in Fig. 2(b) and (d). From the 3D topographic images, we can see that HE-$MAPbI_{3-x}Br_x$ film has a much smoother surface compared with SA-$MAPbI_{2.1}Br_{0.9}$ film. The calculated rec
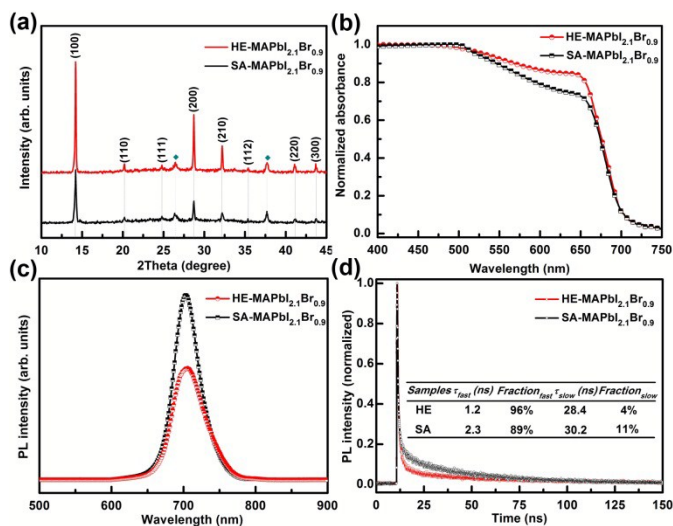
COMMUNICATION

Fig. 3 (a) XRD patterns, (b) normalized UV-vis absorption spectra, (c) PL spectra, and (d) the corresponding normalized time-resolved PL decay curves of $MAPbI_{2.1}Br_{0.9}$ films prepared by halide exchange (HE-$MAPbI_{2.1}Br_{0.9}$) and solvent annealing-induced interdiffusion process (SA-$MAPbI_{2.1}Br_{0.9}$), respectively.

mean square roughness is 18 nm for HE-$MAPbI_{2.1}Br_{0.9}$ film and 56 nm for SA-$MAPbI_{2.1}Br_{0.9}$ film. Therefore, the halide exchange route can realized full surface coverage, large grain size, and homogenous flat $MAPbI_{2.1}Br_{0.9}$ film with a bandgap of 1.75 eV. The film quality is much superior to those for the interdiffusion grown $MAPbI_{2.1}Br_{0.9}$ film, which benefits to weaken the nonradiative recombination of charge carriers in ultimate device.[21, 22]

Fig. 3(a) gives the X-ray diffraction (XRD) patterns of HE-$MAPbI_{2.1}Br_{0.9}$ and SA-$MAPbI_{2.1}Br_{0.9}$ films. It is clear that the diffraction peaks of (100) and (200) lattice planes of HE-$MAPbI_{2.1}Br_{0.9}$ film are stronger than that of SA-$MAPbI_{2.1}Br_{0.9}$ film, which reveals both the improvement of the film crystallinity and the growth of the grains.[4] The normalized absorption spectra of the fabricated HE-$MAPbI_{2.1}Br_{0.9}$ and SA-$MAPbI_{2.1}Br_{0.9}$ films are shown in Fig. 3(b). It can be seen that $MAPbI_{2.1}Br_{0.9}$ films obtained by the two different methods possess similar light absorption properties, with a strong absorption ranging from 400 nm to ~710 nm. Comparable absorption intensity in 400~500 nm is observed, but the absorption of HE-$MAPbI_{2.1}Br_{0.9}$ film is slightly higher than in the range of 550 nm to 710 nm. The stronger light absorption may be related to the high film quality of HE-$MAPbI_{2.1}Br_{0.9}$ film or the little thickness difference of the films (410±5 nm for HE-$MAPbI_{2.1}Br_{0.9}$, 390±8 nm for SA-$MAPbI_{2.1}Br_{0.9}$). Fig. 3(c) gives the photoluminescence (PL) spectra of the samples. An obvious emission peaks at around 700 nm are observed for both samples, which is consistent with their bandgap value. In addition, compared with SA-$MAPbI_{2.1}Br_{0.9}$ film, the PL intensity decreases significantly for HE-$MAPbI_{2.1}Br_{0.9}$ film. As the same surface coverage, the reduced PL intensity can be attributed to the better electron injection into TiO_2 layer from HE-$MAPbI_{2.1}Br_{0.9}$ film.[24] We further performed time-resolved PL decay measurement to undertand the differences of charge extraction and transport in HE-$MAPbI_{2.1}Br_{0.9}$ and SA-

$MAPbI_{2.1}Br_{0.9}$ films, and the corresponding results are presented in Fig. 3(d). The two decay curves were fitted with a two-component exponential decay function containing a fast decay and a slow decay processes. The fast decay process is generally considered to be the result of the quenching of free carriers in the $MAPbI_{2.1}Br_{0.9}$ domains through injection into TiO_2, and the slow decay process to be the result of radiative recombination.[4, 25] As summarized in the insert of Fig. 3(d), the lifetime value of fast decay for HE-$MAPbI_{2.1}Br_{0.9}$ sample is smaller and the corresponding weight fraction of fast decay is higher than those for the SA-$MAPbI_{2.1}Br_{0.9}$ sample. These results effectively confirm the excellent charge dissociation properties of HE-$MAPbI_{2.1}Br_{0.9}$ film.

To understand the advantage of halide exchange route, we fabricated planar-heterojunction solar cells with the device structure of FTO/TiO_2/$MAPbI_{2.1}Br_{0.9}$ /2,2',7,7'-tetrakis (N,N-di-p-methoxy-phenylamine)-9,9'-spirobifluorene (Spiro-MeOTAD)/Ag, as schematically shown in Fig. 4(a). Fig. 4 (b) gives the current density-voltage (J-V) curves of typical devices with HE-$MAPbI_{2.1}Br_{0.9}$ and SA-$MAPbI_{2.1}Br_{0.9}$ films under simulated AM1.5 (100 mW cm^{-2}) illumination, which were measured at forward scan (FS, from short-circuit to open-circuit under the forward bias voltage) and reverse scan (RS, from open-circuit to short-circuit under the forward bias voltage) with a 50 ms scan delay time. Under RS, the device with SA-$MAPbI_{2.1}Br_{0.9}$ film showed the short circuit current density (J_{sc}), the open circuit voltage (V_{oc}), the fill factor (FF), and the PCE to be 16.88 mA cm^{-2}, 1.01 V, 0.52, and 9.55%, respectively. Under FS, the corresponding performance parameters were 16.89 mA cm^{-2}, 0.98 V, 0.49, and 8.11%, respectively. These results indicate that the device with SA-$MAPbI_{2.1}Br_{0.9}$ film have inferior performance including low PCE and serious current hysteresis. In contrast, Under RS, the device with HE-$MAPbI_{2.1}Br_{0.9}$ film showed the J_{sc}, V_{oc}, FF, and PCE to be 18.19 mA cm^{-2}, 1.01 V, 0.69, and 12.67% respectively. Under FS, the performance parameters were extremely close to those for the device under RS, indicating the negligible current hysteresis of the device with HE-$MAPbI_{2.1}Br_{0.9}$ film. To further determine the more real PCE of the fabricated device, the photocurrent value was record as a function of time at a forward bias near its maximum output power point. As shown in Fig. 4(c), the photocurrent density stabilized within seconds to approximately 13.30 mA cm^{-2} at 0.66 V for the device with the SA-$MAPbI_{2.1}Br_{0.9}$ film, yielding stabilized PCE around 8.78 %. In contrast, for the device with HE- $MAPbI_{2.1}Br_{0.9}$ film, the photocurrent density stabilized within seconds to about 15.62 mA cm^{-2} at 0.79 V, yielding stabilized PCE around 12.34 %. Clearly, the device with HE-$MAPbI_{2.1}Br_{0.9}$ film has much superior performance compared with the device with SA-$MAPbI_{2.1}Br_{0.9}$ film. The excellent PV properties of the device with HE-$MAPbI_{2.1}Br_{0.9}$ film are largely related to the high film quality of HE-$MAPbI_{2.1}Br_{0.9}$ film, which significantly reduces the nonradiative recombination and improving the dissociation property of charge carriers.[3, 21, 2] The incident photon conversion efficiency (IPCE) of the fabricated devices were further investigated. As shown in Fig. 4(d), the photocurrent generation started at around 710 nm, in
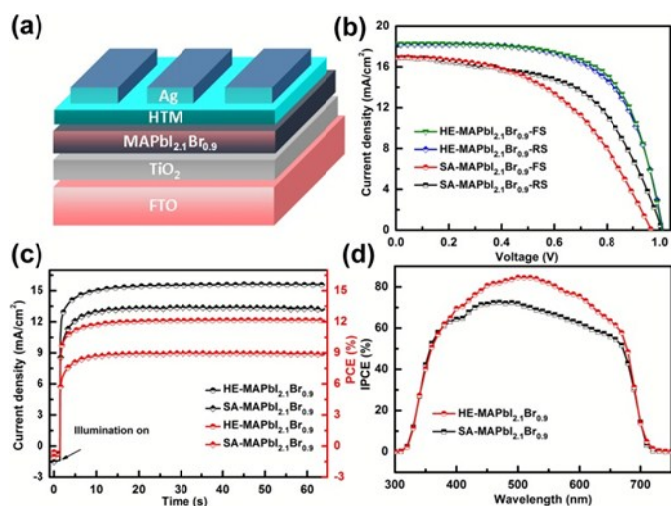
Fig. 4 (a) Schematic device structure of the planar-heterojunction solar cell with $MAPbI_{2.1}Br_{0.9}$ film. (b) Representative J-V curves measured under AM 1.5 simulated sunlight (100 mW/cm^2 irradiance), (c) Stabilized current density and power output measured close to the maximum power point, and (d) IPCE spectra for the devices with $MAPbI_{2.1}Br_{0.9}$ films prepared by halide exchange (HE-$MAPbI_{2.1}Br_{0.9}$) and solvent annealing-induced interdiffusion process (SA-$MAPbI_{2.1}Br_{0.9}$), respectively.

agreement with the estimated bandgap of the $MAPbI_{2.1}Br_{0.9}$ films.[9] The device employed the SA-$MAPbI_{2.1}Br_{0.9}$ film exhibited the IPCE below 65%, yet the device employed the HE-$MAPbI_{2.1}Br_{0.9}$ film gave a remarkable improvement of photocurrent over the whole region, indicating its better photoelectric conversion characteristics. All the above results indicate that the halide exchange route for realizing dense and homogenous flat $MAPbI_{2.1}Br_{0.9}$ film with the bandgap of 1.75 eV can be a facile way to fabricate large-bandgap perovskite solar cells with excellent performance, thus facilitating the development of perovskite-based tandem cells.

In summary, a facile and effective halide exchange method was presented to prepare dense and homogenous flat $MAPbI_{2.1}Br_{0.9}$ film with wide bandgap of 1.75 eV as the light absorber layer in planar-heterojunction solar cell for tandem cell application. Compared to the SA-$MAPbI_{2.1}Br_{0.9}$ film with randomly cumulated nanorod-like structures, the HE-$MAPbI_{2.1}Br_{0.9}$ film composes of large grains and vertically oriented grain boundaries. The planar-heterojunction solar cell based on the high-quality HE-$MAPbI_{2.1}Br_{0.9}$ film showed an optimal PCE of 12.67% with negligible current hysteresis, which is much better than that of the device employed the SA-$MAPbI_{2.1}Br_{0.9}$ film with the same bandgap.

Notes and references

1. H.-S. Kim, C.-R. Lee, J.-H. Im, K.-B. Lee, T. Moehl, A. Marchioro, S.-J. Moon, R. Humphry-Baker, J.-H. Yum, J. E. Moser, M. Grätzel and N.-G. Park, *Sci. Rep.*, 2012, **2**, 591:1-7.
2. M. Liu, M. B. Johnston and H. J. Snaith, *Nature*, 2013, **501**, 395-398.
3. C. Bi, Q. Wang, Y. Shao, Y. Yuan, Z. Xiao and J. Huang, *Nat. Commun.*, 2015, **6**, 7747.
4. W. Zhu, T. Yu, F. Li, C. Bao, H. Gao, Y. Yi, J. Yang, G. Fu, X. Zhou and Z. Zou, *Nanoscale*, 2015, **7**, 5427-5434.
5. G. Xing, N. Mathews, S. Sun, S. S. Lim, Y. M. Lam, M. Grätzel, S. Mhaisalkar and T. C. Sum, *Science*, 2013, **342**, 344-347.
6. M. M. Lee, J. Teuscher, T. Miyasaka, T. N. Murakami and H. J. Snaith, *Science*, 2012, **338**, 643-647.
7. Y. Zhao and K. Zhu, *J. Am. Chem. Soc.*, 2014, **136**, 12241-12244.
8. S. A. Kulkarni, T. Baikie, P. P. Boix, N. Yantara, N. Mathews and S. Mhaisalkar, *J. Mater. Chem. A*, 2014, **2**, 9221-9225.
9. J. H. Noh, S. H. Im, J. H. Heo, T. N. Mandal and S. I. Seok, *Nano Lett.,* 2013, **13**, 1764-1769.
10. C. D. Bailie, M. G. Christoforo, J. P. Mailoa, A. R. Bowring, E. L. Unger, W. H. Nguyen, J. Burschka, N. Pellet, J. Z. Lee and M. Grätzel, *Energy Environ. Sci.*, 2015, **8**, 956-963.
11. J. C. Fan, B. J. Palm and B. Y. Tsaur, *Optimal design of high-efficiency tandem cells*, 1982.
12. R. W. Miles, *Vacuum*, 2006, **80**, 1090-1097.
13. M. Zhang, M. Lyu, H. Yu, J. H. Yun, Q. Wang and L. Wang, Chem.– Eur. J., 2015, **21**, 434-439.
14. K. Cao, J. Cui, H. Zhang, H. Li, J. Song, Y. Shen, Y. Cheng and M. Wang, *J. Mater. Chem. A*, 2015, **3**, 9116-9122.
15. D. Solis-Ibarra, I. Smith and H. Karunadasa, *Chem. Sci.*, 2015, **6**, 613–617.
16. P. Fedeli, F. Gazza, D. Calestani, P. Ferro, T. Besagni, A. Zappettini, G. Calestani, E. Marchi, P. Ceroni and R. Mosca, *J. Phys. Chem. C*, 2015, **119**, 21304-21313.
17. C. Bi, Y. Yuan, Y. Fang and J. Huang, *Adv. Energy Mater.,* 2015, **5**, 1401616
18. D. M. Jang, K. Park, D. H. Kim, J. Park, F. Shojaei, H. S. Kang, J.-P. Ahn, J. W. Lee and J. K. Song, *Nano Lett.*, 2015, 15, 5191-5199.
19. D. Wood and J. Tauc, *Phys. Rev. B: Solid State*, 1972, **5**, 3144.
20. P. Fedeli, F. Gazza, D. Calestani, P. Ferro, T. Besagni, A. Zappettini, G. Calestani, E. Marchi, P. Ceroni and R. Mosca, *J. Phys. Chem. C*, 2015, **119**, 21304-21313.
21. B. Yang, O. Dyck, J. Poplawsky, J. Keum, A. Puretzky, S. Das, N. Ivanov, C. M. Rouleau, G. Duscher and D. B. Geohegan, *J. Am. Chem. Soc.*, 2015, **137**, 9210-9213.
22. Z. Xiao, Q. Dong, C. Bi, Y. Shao, Y. Yuan and J. Huang, *Adv. Mater.,* 2014, **26**, 6503-6509.
23. J. Yan, X. Ke, Y. Chen, A. Zhang and B. Zhang, *Appl. Surf. Sci.,* 2015, **351**, 1191-1196.
24. Z. Zhu, J. Ma, Z. Wang, C. Mu, Z. Fan, L. Du, Y. Bai, L. Fan, H. Yan and D. L. Phillips, *J. Am. Chem. Soc.,* 2014, **136**, 3760-3763.
25. P. W. Liang, C. Y. Liao, C. C. Chueh, F. Zuo, S. T. Williams, X. K. Xin, J. Lin and A. K. Y. Jen, *Adv. Mater.,* 2014, **26**, 3748-3754.